12-3-2018

Covariations of chromospheric and photometric variability of the young Sun analogue HD 30495: evidence for and interpretation of mid-term periodicities

Willie Soon
Harvard-Smithsonian Center for Astrophysics

Victor M. Velasco Herrera
Universidad Nacional Autónoma de México

Rodolfo G. Cionco
Provincia de Buenos Aires - Universidad Tecnológica Nacional

S. Qiu
University of Science and Technology of China

Sallie Baliunas
Harvard-Smithsonian Center for Astrophysics

See next page for additional authors

Recommended Citation

W Soon, V M Velasco Herrera, R G Cionco, S Qiu, S Baliunas, R Egeland, G W Henry, I Charvátová, Covariations of chromospheric and photometric variability of the young Sun analogue HD 30495: evidence for and interpretation of mid-term periodicities, Monthly Notices of the Royal Astronomical Society, Volume 483, Issue 2, February 2019, Pages 2748–2757, https://doi.org/10.1093/mnras/sty3290

Monthly Notices
of the
ROYAL ASTRONOMICAL SOCIETY

MNRAS **483,** 2748–2757 (2019)
Advance Access publication 2018 December 3

doi:10.1093/mnras/sty3290

Covariations of chromospheric and photometric variability of the young Sun analogue HD 30495: evidence for and interpretation of mid-term periodicities

W. Soon,[1]★ V. M. Velasco Herrera,[2]★ R. G. Cionco,[3] S. Qiu,[4] S. Baliunas,[5] R. Egeland,[6] G. W. Henry[7] and I. Charvátová[8]

[1]*Harvard-Smithsonian Center for Astrophysics, Cambridge, MA, 02138, USA*
[2]*Instituto de Geofísica, Universidad Nacional Autónoma de México, Circuito Exterior, C. U., Coyoacán, CDMX, 04510, México*
[3]*Comisión de Investigaciones Científicas (CIC), Provincia de Buenos Aires - Universidad Tecnológica Nacional (UTN), Colón 332, San Nicolás, Buenos Aires, Argentina*
[4]*Department of Geophysics, College of the Geology Engineering and Geomatics, Chang'an University, Xi'an, 710064, China; and Key Laboratory of Geospace Environment, Chinese Academy of Sciences, University of Science and Technology of China, Hefei, 230026, China*
[5]*Retired, Harvard-Smithsonian Center for Astrophysics, Cambridge, MA 02138, USA*
[6]*High Altitude Observatory, National Center for Atmospheric Research, Boulder, CO 80307-3000, USA*
[7]*Center of Excellence in Information Systems, Tennessee State University, Nashville, TN 37209, USA*
[8]*Institute of Geophysics, Academy of Sciences, Praha 4, 141 31, Czech Republic*

Accepted 2018 November 29. Received 2018 November 26; in original form 2018 October 12

ABSTRACT

This study reports the synchronization between the chromospheric and photometric variability at time-scale of about 1.6–1.8 yr as observed for the young, rapidly rotating solar analogue HD 30495. In addition, HD 30495 may be presenting evidence of surface differential rotation at time-scales of about 11 d and 21 d, as well as the sunspot-like decadal cycles at 11–12 yr or so. We apply a new gapped wavelet method of time–frequency analysis for studying the variability in a new composite of the chromospheric *S*-index (1967–2018) and the longest photometric $\Delta(b + y)/2$ index (1993–2018). We discuss and interpret our results in relation to other observed mid-term periodicities roughly of the same time-scales that had been found recently from not only chromospheric and photospheric activity indices but also from coronal X-ray emissions as observed in a considerably large set of stellar samples including those young Sun analogues from the *Kepler* satellite project. Thus, there is an apparent universality of such mid-term activity modulation time-scales as this solar-stellar magnetic phenomenon is well observed directly for a host of solar activity related indices covering the photopsheric, chromospheric, coronal, and even the heliospheric (utilizing the measures of incoming galactic cosmic rays as a probe of activity variations) activity records. This is why we made a further attempt to interpret the results in search of a realistic generation mechanism as well as spatio-temporal persistency of the phenomenon under a wide scenario of dynamo simulations.

Key words: methods: data analysis – stars: activity – stars: chromospheres – stars: individual:HD 30495 .

1 INTRODUCTION

With the advent of more time-continuous observations and numerical dynamo simulations, solar and stellar astronomers and even space physicists are increasingly becoming aware of the solar, stellar, and even heliospheric oscillations that manifest their expressions on the intermediate time-scales that are roughly between one orbital year of the Sun–Earth revolution and the well-known sunspot cycles of roughly 11 yr or so. Those periodicities from 1 to 4 yr are broadly categorized as the quasi-biennial oscillation (QBO) of solar activity (see Howe et al. 2000; Mendoza, Velasco & Valdés-Galicia 2006; Obridko & Shelting 2007; Valdés-Galicia & Velasco 2008;

★ E-mail: wsoon@cfa.harvard.edu (WS); vmv@geofisica.unam.mx (VMVH)

Fletcher et al. 2010; Bazilevskaya et al. 2014, 2016; McIntosh et al. 2015; Gyenge, Ludmány & Baranyi 2016; Olah et al. 2016; Kiss, Gyenge & Erdélyi 2018; Velasco Herrera et al. 2018) and have long been speculated to be associated with the underlying solar dynamo processes. In addition, the correlation or synchronization between solar activity and galactic cosmic rays on QBO time-scales was studied by Bazilevskaya et al. (2014, 2016), Kiss et al. (2018), Velasco Herrera et al. (2018), and those relationships appear to be statistically robust and hence physically meaningful.

In this paper, we seek to further add to the empirical evidence as well as to a better understanding of this phenomenon of mid-term periodicities (MTPs) for the young [i.e. ∼1 Gyr; see table 1 of Egeland et al. (2015)] solar analogue HD 30495 by presenting a new time–frequency wavelet coherence examination of the unique data sets of both the photometric, $\Delta(b+y)/2$ index from the Tennesse State University/Fairborn Observatory Automatic Photometric Telescope Project (Henry 1999) and the chromospheric, Ca II H & K emission *S*-index from the Mount Wilson Observatory HK Project (Wilson 1978; Baliunas et al. 1995) and several other important updated observations [i.e. from the Solar Stellar Spectrograph, SSS, Project at Lowell Observatory (see Hall & Lockwood 1995; Hall, Lockwood & Skiff 2007; Radick et al. 2018; Hall et al. in preparation); the SMARTS Southern HK Project (Metcalfe et al. 2009) at Cerro Tololo Inter-American Observatory; the HARPS Project at La Silla Observatory and the California Planet Search Project (Isaacson & Fischer 2010) at Lick and Keck Observatories].

This young solar analogue HD 30495 has been comprehensively studied and examined by Egeland et al. (2015) including their study of spectral characteristics using periodograms. This work complements Egeland et al. (2015) by focusing strictly on the wavelet time–frequency analyses of the chromospheric and photometric time series as well as important results on the detection of the 1.7 yr MTP using the new gapped wavelet coherence (gWTC) method introduced here.

In addition, we will strive for a fuller understanding of the physical nature of such mid-term oscillations (see Olah et al. 2016; Brandenburg, Mathur & Metcalfe 2017; Katsova et al. 2018; Stefani, Giesecke & Weier). In our brief survey of the latest literature, we found the reports on the detection of periodicity of about 1.6–1.8 yr for not only magnetic but also coronal activity in, e.g. three young solar analogues: ι Horologii (Metcalfe et al. 2010; Sanz-Forcada, Stelzer & Metcalfe 2013; Flores et al. 2017a), KIC 10644253 (Salabert et al. 2016), and 8041424 (Montet, Tovar & Foreman-Mackey 2017). Even more spectacularly, Reinhold, Cameron & Gizon (2017) recently reported the detection of significant amplitude of variability in 3203 stars from the *Kepler* sample with periods ∼0.5–6 yr, covering stars with stellar rotation periods from 1 to 40 d.

Indeed the call for gaining the understanding on the nature of how our Sun varies through the dedicated observations of solar-type stars like HD 30495 has long been anticipated and pioneered some 50 yr ago: (Wilson 1968: p. 221)

'... A vast amount of observational data and theoretical speculation relating to the cyclical solar variation has been accumulated. Nevertheless, it seems very likely that understanding has been severely hampered because all this material relates to a single star with a fixed set of parameters such as age, mass, and surface temperature. It is a reasonable supposition that if analogous cycles could be detected in other stars with different values of the fundamental stellar parameters, the results would be of considerable value in sharpening the theoretical attack on the whole problem.'

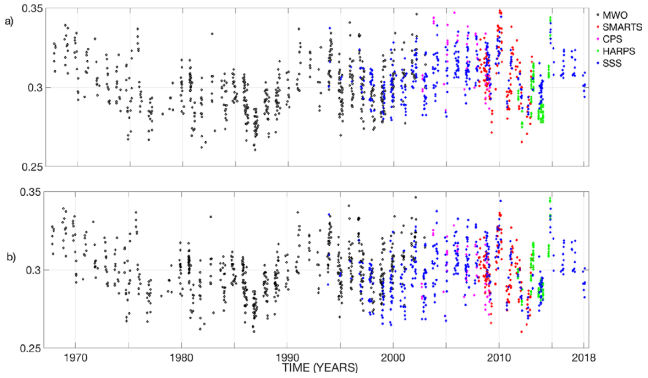

Figure 1. (a) Raw, uncorrected HD 30495 *S*-index values from five different sets of measurement programs (black dots – MWO, red dots – SMARTS, magenta dots – CPS, green dots – HARPS, and blue dots – SSS). (b) The new composite time series *S* for HD 30495 inter-calibrated using equation (3) or (4) based on the chosen reference scale of MWO *S*-index record, from 1967 to 2018.

2 DATA AND METHOD

2.1 Mount Wilson Observatory HK Project and Tennessee State University/Fairborn Observatory Automated Photometric Telescope Project

In this paper, we take full advantage of the unique opportunity, proffered by the newly assembled/compiled data bases recently published in Egeland et al. (2015), in analysing the covariations of the two well-known surface magnetic activity proxies for the young solar analogue HD 30495. Owing to the narrow focus of this study outlined in the Introduction, we will defer to Egeland et al. (2015) and some of our earlier works for the full descriptions of the measurement methods and uncertainties, accuracy in record calibrations as well as the known physical characteristics and magnetic activity variation for this star.

The Strömgren photometric $\Delta(b+y)/2$ time series for HD 30495 analysed in this paper covers the full interval from 1993 to 2018. The *S* time series contains data from six different sources. The measurements come from the original Mount Wilson survey, the SSS program at Lowell Observatory, the SMARTS Southern HK survey, the HARPS survey, the Hamilton Spectrometer at Lick Observatory, and the High Resolution Echelle Spectrometer (HIRES) instrument at Keck Observatory (i.e. the last two observations are part of the California Planet Search, CPS, project). In Fig. 1a, we present the raw, uncalibrated and uncorrected *S*-index for these five different groups of time series records (black dots – MWO, red dots – SMARTS, magenta dots – CPS, green dots – HARPS, and blue dots – SSS). The statistical characteristics (mean value and standard deviation) of the measurements obtained by the different instruments are shown in Table 1.

2.2 Calibration algorithm for measurements of *S*-index made by different instruments

Indeed in order to better understand both the time-averaged and time-variable nature of solar and stellar activity, one must have continuous measurements for a long interval of time. Unfortunately,

Table 1. Statistical characteristics for *S*-index from different instrumentations and projects.

S-index time series	Statistical Characteristics		
	Mean value	Standard deviation	Calibration factor
MWO	0.299	0.0158	1
SSS	0.3076	0.0127	1.2441
SMARTS	0.3078	0.0169	0.9349
CPS	0.316	0.0164	0.9634
HARPS	0.2973	0.0162	0.9753

this is not possible because nearly all instruments (sensors) have a finite operating time. Furthermore, it is not possible to replace one instrument with another without changes in the process of data acquisition because there are no two detectors that are the same. In addition, data acquisition electronics may change. Different instrument models have different algorithms in the acquisition of the data. Each instrument has its own calibration factor, among other difficulties.

This is why it is necessary to make a composite record of overlapping, calibrated measurements obtained with different instruments. If there is a set of instruments, which measure the same parameter (for example S_i, where i means the instrument number) of a celestial body and it is required to make a data composite ($S^{'}$) from all different instruments, then it is necessary to search for the correction function (ϕ)

$$S' = \phi(S_i) \tag{1}$$

By measuring the same parameter and being 'almost the same type of instrument', a first approximation of the correction function (ϕ) is a linear function

$$S' = \phi(S_i) \simeq K S_i + b \tag{2}$$

The main problem of equation (2) is to find the parameters K and b with relatively high accuracy. These parameters can be found through different artificial intelligence modelling-verification techniques. If a full calibration information is not available, then the statistical method may be used to find the parameters K and b. These parameters will be deduced using the methodology proposed by Velasco Herrera, Mendoza & Velasco Herrera (2015) that attempted to homogenize and standardize all the measurements of the different instruments relative to the reference Mount Wilson instrumental scale.

1. The first step that Velasco Herrera et al. (2015) proposed is that each of the data sets obtained with different instruments can be centralized to have a mean value equal to zero and normalized to have standard deviation equal to one

$$\hat{S}_i = \frac{S_i - <S_i>}{\sigma_i},$$

where subscript i denotes the measurements from four other instruments (1 = SSS, 2 = SMARTS, 3 = CPS, and 4 = HARPS), $<S_i>$ is the mean value, and σ_i is the standard deviation.

2. The second step in the recalibration of the data is to multiply the centralized and standardized variables by the standard deviation of the data chosen as a reference. In our case we will use the measurements derived from the original Mount Wilson survey (i.e. with subscript m).

3. The third step is to add a term that is equal to the mean value of the data chosen as a reference ($<S_m>$)

$$S'_i = \sigma_m \hat{S}_i + <S_m>. \tag{3}$$

The first term of equation (3) represents the stability of the conditions during the entire calibration and the second term is a corrected calibration factor. Equation (3) can be rewritten as follows:

$$S'_i = \frac{\sigma_m}{\sigma_i}[S_i] + \left[<S_m> - \frac{\sigma_m}{\sigma_i}<S_i>\right]. \tag{4}$$

From equation (2), equation (4) can be written as follows:

$$S'_i = K_i S_i + b_i,$$

where the calibration factor $K_i = \frac{\sigma_m}{\sigma_i}$ and $b_i = <S_m> - \frac{\sigma_m}{\sigma_i}<S_i>$.

The new composite time series S for HD 30495 constructed here contains data from the original Mount Wilson survey (S_m) and the data calibrated from four different groups (S_i) using equation (3) or (4). The result is shown in Fig. 1b. We will use this composite *S*-index record from 1967 to 2018 for the spectral analysis in this paper. We note the application of equation (3) or (4) rescales the other data sets to have consistent means and standard deviations compared to the MWO *S*-index record. We observe only very minor differences from the previous compositing method used in Egeland et al. (2015). In addition, the algorithm described above can be applied for compositing of any data set regardless of how they were measured.

2.3 Gapped wavelet transform

In this paper, we will apply our new gapped wavelet transform method of time–frequency analysis to reveal more fully the spectral characteristics for the Mount Wilson Observatory HK Project's instrumental chromospheric *S*-index from 1967 to 2018 and the Tennessee State University/Fairborn Observatory's Strömgren photometric $\Delta(b + y)/2$ index from 1993 to 2018 as well as the covariations of the two stellar activity indices. Although there are extensive works and physical arguments to support our interpretation here: throughout this study, we will assume, for simplicity, that the record of *S*-index represents the chromospheric heating from magnetic variability as captured by the relatively bright regions called plages on the Sun and sun-like stars and the record of $\Delta(b + y)/2$ index represents the photopsheric variability as captured and modulated by dark stellar magnetic spot regions. To the best of our knowledge, this paper is also the first to compute the gWTC (see discussion below) between the chromospheric and photometric variations for HD 30495 and hence allows us to reveal the physical nature of the bright plage–dark spot relations covering the rotational to sunspot-like decadal time-scales.

The wavelet spectra of astrophysical, astronomical, or geophysical phenomena allow us to: (a) identify the intrinsic properties of the phenomenon, (b) determine the characteristics of the phenomenon's source, and (c) determine the interaction between the phenomenon and its source and/or the interaction between the phenomenon and the environment/medium involved. Classical spectral analysis requires that the time series being analysed has a uniform sampling cadence with no gaps. There are several problems when analysing a time series with gaps using a standard wavelet transform. In addition, the most restrictive requirement is that the data points must be equidistant temporally, i.e. with equal sampling times.

Unfortunately, data gaps in astronomical, astrophysical, or geophysical data bases are ubiquitous. This is mainly because those irregular measurements were created with data from different observational opportunities and constraints as well as involving various instruments and methodologies. Also, in astronomical observations, one is faced especially with time-limited observations leading to stellar activity records that are often occupied by irregular obser-

vational gaps. Moreover the measurements contain errors, missing data, there may be even problems related to lost data as well as unregistered data. This is why Frick et al. (1997, 1998) has long anticipated the proper handling of such practical issues by introducing the so-called data-adaptive 'gapped wavelet' to compute the wavelet transform that satisfied the admissibility condition in order to minimize the common aliasing problems arising from irregularly spaced data gaps. We have previously made full use of such an important innovative method of analysis for the Mount Wilson HK Project data records (see Frick et al. 1997; Soon, Frick & Baliunas 1999).

Frick et al. (1997, 1998) defined the gapped wavelet transform ($\mathcal{W}_g$) as follows:

$$\mathcal{W}_g^{f}(t,s) = \sqrt{\frac{1}{s\ C(s,t)}} \int_{-\infty}^{\infty} \psi'^{*}(t',t,s) f_g(t')\,\mathrm{d}t' \tag{5}$$

with

$$\psi'(t',t,s) = \left[h\left(\frac{t'-t}{s}\right) - C(s,t)\right] \Phi\left(\frac{t'-t}{s}\right) G(t'),$$

$$C(s,t) = \frac{\int_{-\infty}^{\infty} h\left(\frac{t'-t}{s}\right) \Phi\left(\frac{t'-t}{s}\right) G(t')\,\mathrm{d}t'}{\int_{-\infty}^{\infty} \Phi\left(\frac{t'-t}{s}\right) G(t')\,\mathrm{d}t'},$$

$$G(t) = \begin{cases} 1, & \text{if the signal is registered} \\ 0, & \text{no signal, lost data or not reported} \end{cases}, \tag{6}$$

where ψ is the wavelet basis function, $f_g(t)$ is a gapped time series, $*$ is the complex conjugate, s is the scale, and t is the time. We adopt the Morlet wavelet because it is a complex function (Torrence & Compo 1998) that allows one to reconstruct the phase of the signal and because of its high resolving power in the frequency/periodicity space. In this case, the function Φ and h is given by: $\Phi(t) = e^{(-t^2/2)}$, $h(t) = e^{iw_o t}$, with $w_o = 6$. In the central panels of Figs 2–4, the calculated local wavelet power spectral density (LWPSD), in arbitrary (normalized) units, is shown adopting the red–green–blue colour scales.

We add that the algorithm we adopted in order to accelerate the calculations of the wavelet transform (i.e. similar to the computation of a fast Fourier transform) requires that the number of data be of length 2^N. As this condition is not fulfilled regularly, one way to solve this problem is to artificially fill the time series until the next power of two with zeros (for other possibilities, see Meyers, Kelly & O'Brien 1993). This technique can cause false or spurious periodicities. Therefore, it is necessary to indicate for the LWPSD plotted in Figs 2–4, the possible areas where these periodicities could be identified. It is precisely the cone of influence (COI) that shows these edge effects in the LWPSD (U-shaped curves marked in Figs 2–4). In the standard wavelet analysis (i.e. time series without gaps, e.g. Torrence & Compo 1998), the extension of the COI depends on the number of data in the time series and the choice mother wavelet function. In the case of gapped time series, according to equation (6), the COI does not depend on the number of gaps since we never weigh in the gaps in the wavelet calculation. It should be further noted that the gapped wavelet algorithm we applied does not involve any arbitrary interpolation or filling of data gaps.

We also plotted the global time-averaged wavelet in the left-hand panels of Figs 2–4. In order to mark the periodicities that have equal to or greater than 95 per cent confidence level (i.e. red dashed lines in the left-hand panels), we use the autoregressive AR (1) process with correction factor α (Gilman, Fuglister & Mitchell 1963). The values of the correlation factor for the *S*-index (1967–2018) and the photometric $\Delta(b+y)/2$ index (1993–2018) time series are $\alpha_1 = 0.9934$ and $\alpha_2 = 0.9806$, respectively.

In this work, we use a new implementation of the gapped wavelet squared coherency ($\mathscr{R}_g^2$) technique/algorithm to study the degree of syncrhonization between the chromospheric *S*-index and photometic $\Delta(b+y)/2$ index time series of the young Sun analogue HD 30495. $\mathscr{R}_g^2$ is a dimensionless frequency matrix and this matrix varies between zero and one. We define $\mathscr{R}_g^2$ as follows in order to better reveal the degree of frequency synchronization of two phenomena ($\mathscr{X}$, $\mathscr{Y}$) that are connected under the broad theme of solar and stellar magnetism and their activity variations:

$$\mathscr{R}^2(t,s) = \left\langle \left| \mathscr{W}_g^{\mathscr{X}\mathscr{Y}}(t,s) \right|^2 \right\rangle \ominus \left\langle \left| \Omega_g(t,s) \right|^2 \right\rangle \tag{7}$$

with

$$\mathscr{W}_g^{\mathscr{X}\mathscr{Y}}(t,s) = \mathscr{W}_g^{\mathscr{X}}(t,s) \otimes \mathscr{W}_g^{*\mathscr{Y}}(t,s) \tag{8}$$

$$\left\langle \left| \Omega_g(t,s) \right|^2 \right\rangle = \left\langle s^{-1} \left| \mathscr{W}_g^{\mathscr{X}}(t,s) \right|^2 \right\rangle \otimes \left\langle s^{-1} \left| \mathscr{W}_g^{\mathscr{Y}}(t,s) \right|^2 \right\rangle, \tag{9}$$

where $\otimes$ and $\ominus$ are the Hadamard multiplication of matrices and the Hadamard division of matrices, respectively and $\langle . \rangle$ represents the temporal and frequency average (e.g. Torrence & Compo 1998; Torrence & Webster 1999; Grinsted, Moore & Jevrejeva 2004; Velasco Herrera et al. 2017). One of the biggest problems in studying the cross-wavelet and wavelet coherence is that the problem involves matrix algebra that is very different from that normally taught in traditional matrix courses. This is why we present the formula in the Appendix that show that the gapped cross-wavelet is the result of the Hadamard multiplication of matrices, and the gWTC is the result of the Hadamard division of matrices.

Equation (8) (i.e. $\mathscr{W}_g^{\mathscr{X}\mathscr{Y}}(t,s)$) is the gapped cross-wavelet and shows the degree of similarity and differences frequency between two physical phenomena (e.g. the chromospheric and photometric variability) and allows to find the relevant characteristics of the physical system where these phenomena are developed as well as to find their patterns of variation (for example in the Sun analogue HD 30495). It also allows to find the relative phase between two phenomena and reduces the noise of two signals [e.g. *S*-index and $\Delta(b+y)/2$ index time series]. Equation (9) (i.e. $\langle |\Omega_g(t,s)|^2 \rangle$) represents the product of gapped wavelet power spectra of two phenomena.

The instantaneous relative phase difference in the gapped wavelet coherency (ϕ_g), the global gapped time-averaged wavelet coherence spectrum ($G_{\mathscr{R}_g^2}$), and the global gapped frequency-averaged wavelet coherence spectrum (G_{ϕ_g}) are defined, respectively, as follows:

$$\phi_g(t,s) = tan^{-1}\left(Im\left[\mathscr{W}_g^{\mathscr{X}\mathscr{Y}}(t,s)\right] \ominus Re\left[\mathscr{W}_g^{\mathscr{X}\mathscr{Y}}(t,s)\right]\right) \tag{10}$$

$$G_{\mathscr{R}_g^2} = \sum_t \mathscr{R}_g^2(t,s) \tag{11}$$

$$G_{\phi_g} = \sum_{\phi} \phi_g(t,s) \tag{12}$$

3 RESULTS AND INTERPRETATIONS

Fig. 2 shows the result for our new gapped wavelet analysis of the chromospheric *S*-index activity variations covering the full 51 yr interval of the record. We can easily confirm the existence, albeit with notable time intermittency, of the intermediate scale periodicity at

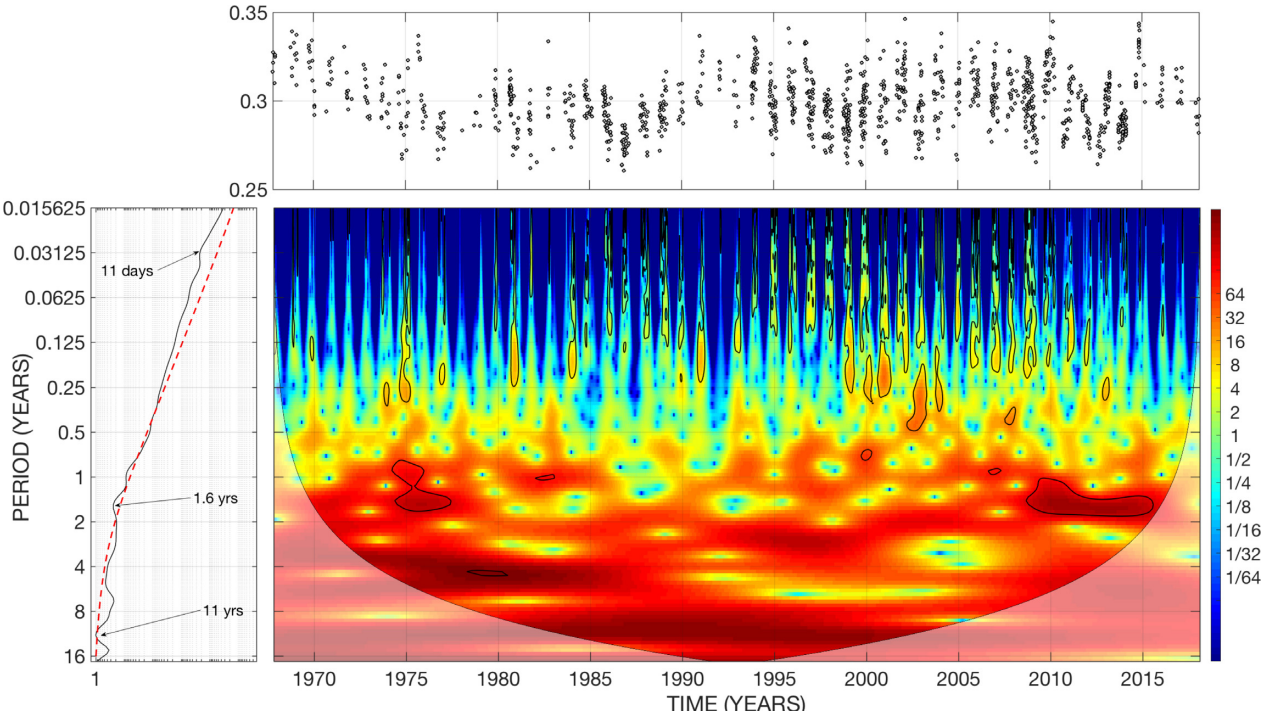

Figure 2. Time–frequency gapped wavelet spectrum of chromospheric *S*-index variations for the young Sun analogue HD 30495 from 1967 to 2018. In the central panel, the calculated local wavelet power spectral density in arbitrary units is shown adopting the red–green–blue colour scales. The cone of influence shows the possible edge effects in the LWPSD (see the text for further explanation). The global time-averaged wavelet is shown in the left-hand panel with the red dashed line indicating the 95 per cent confidence level.

roughly 1.6 yr. In addition, Fig. 2 reveals that the decadal-like variations have possibly divided peaks at 11 yr and another oscillation at > 20 yr (not shown directly since the oscillation is well outside of COI), respectively. We propose that this tentative finding is consistent with the results presented by Egeland et al. (2015) where those authors showed that HD 30495 may contain decadal-like periods between 9.6 and 15.5 yr.

It is clear that despite having this unique ground-breaking record of 51 yr of dedicated monitoring of this young Sun analogue, we are nowhere near the ideal observational record length to have full confirmation or resolution of its decadal-like activity cycles since the oscillation at decadal and bidecadal time-scales are pretty much still well outside of the COI for a confident detection. On the other hand, in defense of a proper physical interpretation, one may counter that the COI is a statistical concept and may be overly restrictive under our current calculations (see the earlier discussion related to the practical procedure of padding of endpoints of time series records with zeros).

Fig. 3 shows the result for our gapped wavelet analysis of the photometric $\Delta(b + y)/2$ index activity variation for the more limited interval of 1993–2018. When studying the photometric data series in Fig. 3, the reader should keep in mind that the data are plotted on a relative magnitude scale where higher values imply lower brightness. Despite the limitation, the wavelet spectrum clearly yields signatures of the activity modulation at the two key time-scales of 1.6 yr and 11.5 yr, respectively. This direct confirmation from another independent observational record adds a significant confidence that we are deciphering a true physical phenomenon of magnetic variability in HD 30495 as shown in Fig. 2 for *S*-index time series. Here we may note that indeed the power of adopting a gapped wavelet analysis is for us to recognize the detection of the 1.6 yr oscillation in Fig. 3 for a pertinent instant of time (local scale) rather than strictly for all time based on the global time-averaged spectra alone (relative to the chosen red-noise spectrum).

A detailed examination of the results from Figs 2 and 3 further reveal that the 1.6 yr oscillation is modulated by the longer decadal-like oscillations perhaps offering the empirical evidence that the two oscillations are not completely independent from each other. It may not be entirely surprising to observe that the detection of the mid-term oscillation of 1.6 yr is more clearly resolved during the weaker activity phase of the decadal-like oscillation as can be noted from Figs 2 and 3. This particular observational evidence should be able to help constrain the theoretical underpinning from dynamo studies.

Fig. 4 shows the gWTC spectrum revealing the interrelationship between the chromospheric *S*-index and photometric $\Delta(b + y)/2$ index from 1993 to 2018. The spectrum is quite informative in that one can observe the clear covariation and modulation ranging from rotational time-scales of 11 d to the mid-term oscillations of 1.6–1.8 yr and the sunspot-like decadal time-scales. From the figure, one can deduce that the phase coherence of the covariation at say 1.6–1.8 yr is complex and non-linear. But one can also observe a quasi-continuous modulation from the 2–3 yr time-scale at the beginning of the record evolving to the more continuous modulation at 1–2 yr time-scale. On the longest detected oscillations of roughly 11 yr, we note that the sense of the covariations on this scale is fully consistent with the spot-dominated variability patterns with the wavelet coherence results show an in-phase covariation in that high *S* activity corresponding to high relative $\Delta(b + y)/2$ magnitudes. This behaviour is typical for young solar analogues like HD 30495, but opposite of older stars like the Sun now. We note that the chromospheric–photometric interrelations obtained here for HD

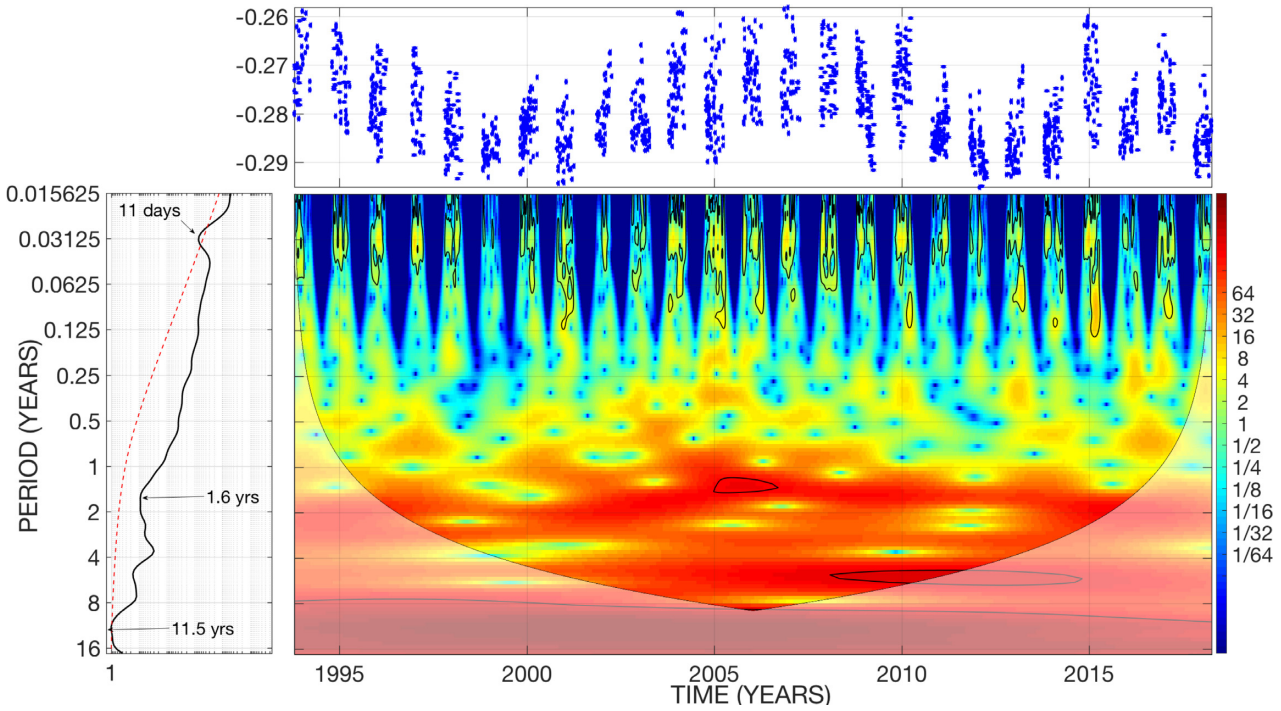

Figure 3. Time–frequency gapped wavelet spectrum of differential photometry $\Delta(b+y)/2$ index variations for the young Sun analogue HD 30495 from 1993 to 2018. Each panel presents similar information as described in Fig. 2. In addition, readers should also be reminded that when studying the photometric data series in this figure that the differential photometric data are plotted on a magnitude scale where higher values imply less flux or weaker starspot activity in contrast to the *S*-index values shown in Figs 1 and 2.

30495 are fully consistent and can complement the new deduction by Reinhold et al. (in press) on how a sun-like star evolves from the stage of spot-dominated bulk light output emission characteristics until it reaches about 2.55 Gyr of age when faculae-dominated characteristics takes over. However, without a physical model, we do not assign any further significance or interpretation to both studies. But a comparison and contrast with the artificial example shown in Fig. A1 allow an added confidence that the MTP phenomenon observed on HD 30495 is worthy of physical interpretation.

The global phase indicator (right-hand panel of Fig. 4) shows that, for periodicities less than one year, the phase is stochastic most likely owing to the intrinsic dispersion of the data in the gapped time series. Such dispersion could be provoked in the wavelet function of adaptive Morlet for the time series with gaps because of not having a high enough time resolution in the local phase of the coherence function. In addition there are abrupt changes in the spectral power caused by these gaps and the dispersion of the data. The global relative-phase for the 1.7 yr oscillation is varying between 0 (in-phase) and $\pi/2$ for periodicities larger than one year. The bottom panel of Fig. 4 shows that the instantaneous phase (black dashed line) for this oscillation between the *S*-index and photometric index is nearly in-phase between 1993 and 1998. During the time interval from 1998 to 2006, the phase plot shows that the relationship is complex between these two magnetic activity indices. After 2006 and until 2018 the relationship is roughly linear again. Moreover, the coherence function (blue curve) shows that coherence in the periodicity of 1.7 yr in time has a modulated covariance with a decadal time-scale. One can, however, also observe that mid-term oscillation of 1.7 yr is modulated by decadal scales that are not single-valued oscillations but instead pulsed with varying lengths of 7–12 yr.

In Fig. 4, we also wish to point out the possibility of the simultaneous detection of two rotational time-scales of covariation at 11 and 21 d for HD 30495. This possibility of detecting two distinct rotational modulations is also hinted especially in Fig. 3. Although our data records are still rather sparse and incomplete, we may support our interpretation using a real-life example showing a similar covariability in the sunspot and 10.7 solar radio flux records as shown in Fig. A2. It is clear that no firm interpretation is possible at this time, but our result in Fig. 4 may plausibly suggest the detection of another rotational modulation at 21 d time-scale for the surface magnetic features at higher latitudes. Lanza and colleagues have recently reported evidence for differential rotation in Sun-like stars and are contemplating their interpretations (see e.g. Lanza et al. 2009; das Chagas et al. 2016). Our results are also not inconsistent with the recent detection of latitudinal differential rotation, using the asteroseismological measurements of stellar convection zones, in 13 out of 40 sun-like stars where the stars' equators rotate about twice as fast as their midlatitude zones (Benomar et al. 2018).

Broadly speaking, Brandenburg et al. (2017) proposed that both the 'short' and 'long' periods of stellar activity cycles can coexist and that those shorter 1–3 yr (i.e. which we called intermediate length or 'mid-term' cycles throughout this paper) cycles can be interpreted in terms of the near-surface dynamo processes where as the longer decadal-like periods are a result of the dynamo mechanims involving deeper layers of the Sun and stars. The former dynamo mechanism is normally associated more with the so-called turbulent dynamo processes and hence may offer a natural explanation for the empirical evidence for the intermittency of the 1.7 yr oscillations throughout the observational records. Such interpretations are rather consistent with the observational results and discussion in Olah et al. (2016). Those authors offered explanations of shorter

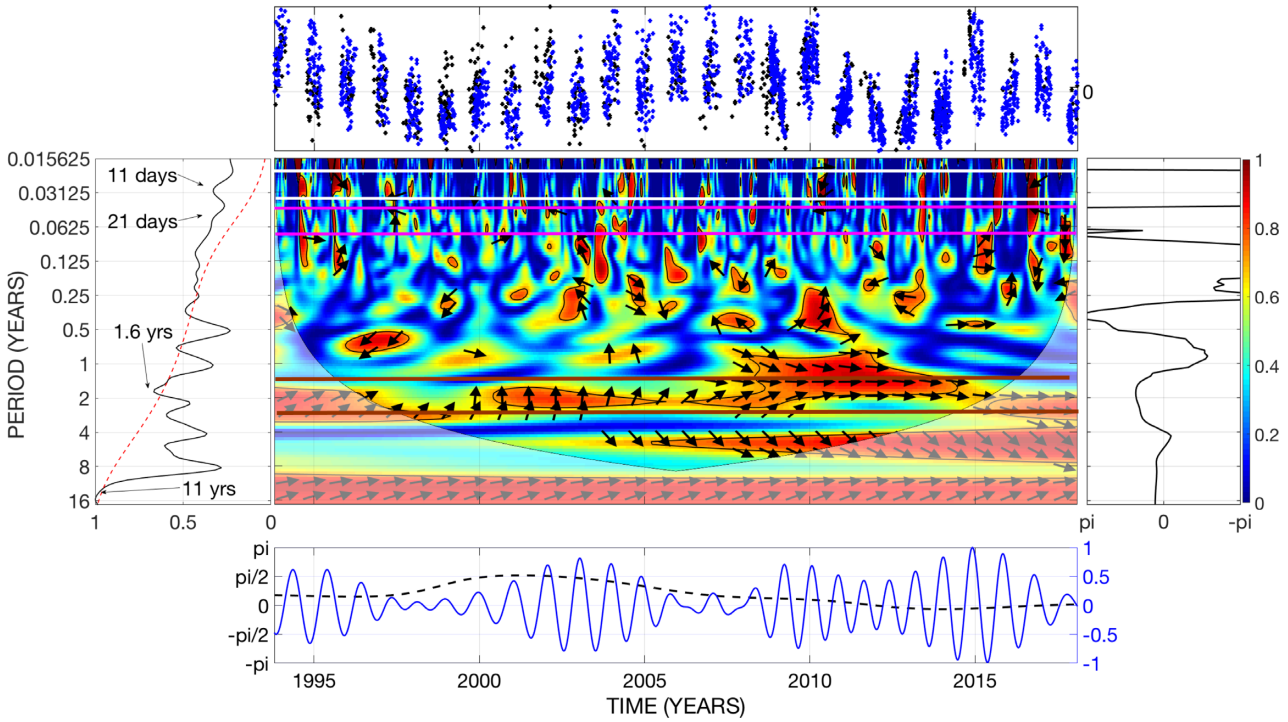

Figure 4. Time–frequency gapped wavelet coherency spectrum of the covariations of chromospheric *S*-index (black dots in top panel) and photometric $\Delta(b + y)/2$ index (blue dots in top panel) for the young Sun analogue HD 30495 on the common interval from 1993 to 2018. The central panel shows the gWTC power adopting the red–green–blue colour scales. The value of one (red colour) indicates highest (perfect)-degree of frequency covariance (synchronization) between *S*-index and photometric $\Delta(b + y)/2$ index time series. The value zero (blue colour) indicates that there is no synchronization between these two phenomena. The black arrows indicate the relative phase of the synchronization. The orientations from left to right (→) and from right to left (←) indicate that there is a linear, in-phase and antiphase, synchronization at a certain frequency between these two phenomena. Any other orientation means that there is a complex, non-linear synchronization. The left-hand panel shows the global gapped time-averaged wavelet coherence spectrum with the red dashed line representing the 95 per cent significance level. The panel on the right shows the global gapped frequency-averaged wavelet coherence spectrum. The bottom panel shows the coherence function of 1.7 yr scale (blue continuous line) and the instantaneous phase relative for this same period (black dashed line). The contrast with the artificial example shown in Fig. A1 informs that the detection of the strong mid-term covariations at 1.6–1.8 yr is significant and physically meaningful. Furthermore, we also remark on the possible detection for two modulations at rotational time-scales of about 11 d and 21 d, respectively.

time-scale periods of stellar activity to be originating from strong field and a relatively thin tachocline while the longer decadal-like cycles are a result of weaker field with thicker tachocline.

Early on Mendoza et al. (2006) reasoned that it is difficult to imagine that how the solar MTP can remain in phase along the journey from the solar convective zone to photosphere if this frequency is to have similar explanation as the 11 yr sunspot cycles generation from the deep-seated tachocline. If the genesis of the 1–4 yr variations is truly from within the tachocline depth, then the convection zone must somehow act effectively as an amplifier in order for the MTP to persist till it reaches the solar surface. The solar MTPs of 1.7 yr have not been registered in the tachocline, but one cannot dismiss the idea entirely [see e.g. fig. 3 of the original observations by Howe et al. (2000) and the theoretical model and frameworks discussed by Dikpati et al. (2018)]. In a different interpretation framework, both MTP and 11 yr sunspot activity cycles could simply be generated in the topmost, upper layers of the convective zone so that the signals could more easily be preserved in phase and thus more conveniently observed in surface magnetic activity indices. Benevolenskaya (1995), based on measurements of surface magnetic fields, found that low-frequency solar dynamo waves with a 22 yr periodicity can coexist with a quasi-biennial (i.e. roughly 1 to 3 yr) period. Furthermore, in an updated study, Benevolenskaya (2001) proposed that QBO variations can be observed in the helicity of solar magnetic fields [i.e. as deduced from fig. 1 of the observational study by Zhang & Bao (1998) which in turn can be updated from, e.g. fig. 6 in Zhang & Yang (1998)] may be generated in the subsurface regions owing to either radial or latitudinal shears of the angular velocity from the influence of erupted magnetic fields of the main solar activity cycles.

Recently, McIntosh et al. (2015) offerred an empirical evidence-based interpretation of magnetic variations on shorter periods than the nominal 11 yr sunspot cycles on the Sun in terms of magnetic latitudinal band interactions and instabilities causing and maintaining the appearance of a host of magnetic oscillation phenomena (i.e. surges of magnetism). Those authors highlighted the detection and explanation of those MTP that cover observational indices from sunspots, flares, and coronal mass ejections. In this framework emphasizing the dynamics of magnetic fluxes and their evolution and propagation, McIntosh et al. (2015) highlighted the primary importance of the termination point for magnetic flux cancellation and renewal near the solar equator as the key fiducial time constant for the solar activity cycles rather than the more artificial constructs from maxima and minima of sunspot numbers. Although we cannot be sure if this explanation may apply for the empirical evidence shown in Figs 1, 2, and 3 for the young solar analogue HD 30495, we do think that the interpretation by McIntosh et al. (2015), when applied to magnetic field for smaller spatial scales than say coronal holes and sunspots, may be relevant or directly applicable for studying HD 30495. The updated numerical simulations by Dikpati

et al. (2018) offer a very exciting interpretation of the so-called solar 'seasons', as quasi-periodic bursts/surges of activity with periods ranging widely from 2 to 20 months that are rather similar to the identified MTP of 1.6–1.8 yr emphasized in this paper for HD 30495.

Stefani et al. (2018a) have shown that Tayler–Spruit type dynamos (with the Ω-effect produced traditionally by solar-like differential rotation profiles) are more susceptible to synchronization from external tidal forcing from solar system planets than say the more traditional Babcock–Leighton type dynamos. This is achieved via the intrinsic helicity oscillation of the current-driven Tayler instability as externally synchronized by the low-amplitude 11 yr tidal forcing of Venus–Earth–Jupiter (see e.g. Cionco & Soon 2015; Stefani et al. 2016). The follow-up numerical investigation by Stefani et al. (in preparation) adopting the Tayler–Spruit dynamo model has indeed found the emergence of MTP (see figs 12 and 13 of that paper) in the simulated magnetic fields as manifested in terms of the observed double-peaks phenomenon as recently elaborated by Karak, Mandal & Banerjee (2018). In this early stage of our research we do not assign any particular significance to the Sun-planets interaction for the interpretation of the solar and stellar magnetic activity variations, but a recent examination by Canto Martins et al. (2011), Flores et al. (2017b), and France et al. (2018) cannot find or confirm any clear relation of chromospheric activity and planetary parameters. On the other hand, other more positive evidence is also available and actively being discussed and debated in the literature (e.g. Poppenhaeger & Wolk 2014; Lanza 2014; Lanza 2018). Here we simply wish to add the fact that Cionco & Pavlov (2018) have recently introduced a comprehensive orbital framework for interpreting oscillations or periodicities in Earth geological and climatic records ranging from interannual (i.e. Venus–Earth synodic period; see e.g. Charvátová 2007) through multimillennial (i.e. Uranus–Neptune great inequality; see e.g. Soon et al. 2014) time-scales and that this framework could be adaptable for any star and planetary system. Furthermore, although it is known that debris discs have been detected around HD 30495 (Greaves, Wyatt & Bryden 2009, 2014), and direct confirmation of Earth- or Venus-sized planets around HD 30495 may still be beyond the current state of the art (e.g. Howard & Fulton 2016). At this early stage of investigating the physical nature of mid-term oscillations, we must emphasize that the Sun-planets interaction framework we are proposing here are merely for intellectual curiosity. Therefore, we do not preclude the well-noted relationship between cycle period and instrinsic properties like rotation that are better established for the inactive branch discussed by several previous authors (i.e. Soon, Baliunas & Zhang 1993; Brandenburg, Saar & Turpin 1998; Böhm-Vitense 2007; Olah et al. 2016; Brandenburg et al. 2017; Egeland 2017; however, see fig. 9 in Montet et al. 2017 for the relatively large scatter within the stellar rotation and activity cycle period relation).

ACKNOWLEDGEMENTS

We thank Jeff Hall for contributing the most updated *S*-index data series for HD 30495 based on the Lowell Observatory SSS instrument. We are very grateful for Peter Frick's critical comments and suggestions, which have led to certain improvements of our manuscript. RE is funded by the NCAR Advanced Study Program Postdoctoral Fellowship. The National Center for Atmospheric Research is sponsored by the National Science Foundation. GWH acknowledges long-term support from NASA, NSF, Tennessee State University, and the State of Tennessee through its Centers of Excellence Program. VMVH acknowledges the support from CONACyT-180148 grant. WS's work was partially supported by the Smithsonian Astrophysical Observatory grants with proposals ID: 0000000000003010-V101 and 0000000000004254-V101.

REFERENCES

Baliunas S. L. et al., 1995, ApJ, 438, 269
Bazilevskaya G., Broomhall A. M., Elsworth Y., Nakariakov V. M., 2014, Space Sci. Rev., 186, 359
Bazilevskaya G. A., Kalinin M. S., Krainev M. B., Makhmutov V. S., Svirzhevskaya A. K., Svirzhevsky N. S., Stozhkov Y. I., 2016, Cosm. Res., 54, 171
Benevolenskaya E. E., 1995, Sol. Phys., 161, 1
Benevolenskaya E. E., 2001, Sol. Phys., 191, 247
Benomar O. et al., 2018, Science, 361, 1231
Böhm-Vitense E., 2007, ApJ, 657, 486
Brandenburg A., Saar S. H., Turpin C. R., 1998, ApJ, 498, L51
Brandenburg A., Mathur S., Metcalfe T. S., 2017, ApJ, 845, 79
Canto Martins B. L., das Chagas M. L., Alves S., Leao I. C., de Souza Neto L. P., de Medeiros J. R., 2011, A&A, 530, A73
Charvátová I., 2007, Ann. Geophsicae, 25, 1
Cionco R. G., Pavlov D. A., 2018, A&A, 615, A153
Cionco R. G., Soon W., 2015, New Astron., 34, 164
das Chagas M. L., et al., 2016, MNRAS, 463, 1624
Dikpati M., McIntosh S. W., Bothun G., Cally P. S., Ghosh S. S., Gilman P. A., Umurhan O. M., 2018, ApJ, 853, 144
Egeland R., 2017, PhD thesis, Montana State Univ.
Egeland R., Metcalfe T. S., Hall J. C., Henry G. W., 2015, ApJ, 812, 12
Fletcher S. T., Broomhall A. M., Salabert D., Basu S., Chaplin W. J., Elsworth Y., Garcia R. A., New R., 2010, ApJ, 718, L19
Flores M. G., Buccino A. P., Saffe C. E., Mauas P.J. D., 2017a, MNRAS, 464, 4299
Flores M. G., Buccino A. P., Saffe C. E., Mauas P.J. D., 2017b, Bull. Asociacion Argentina de Astronomia, 59, 22
France K., Arulanantham N., Fossati L., Lanza A. F., Linsky J. L., Redfield S., Lyold R., Schneider C., 2018, 'Ultraviolet activity levels of G, K, and M dwarf exoplanet host stars', American Astronomical Society Meeting #231
Frick P., Baliunas S. L., Galyagin D., Sokoloff D., Soon W., 1997, ApJ, 483, 426
Frick P., Grossmann A., Tchamitchian W., 1998, J. Math. Phys., 39, 4091
Gilman D. L., Fuglister F. H., Mitchell J. M., Jr., 1963, J. Atmos. Sci., 20, 182
Greaves J. S., Wyatt M. C., Bryden G., 2009, MNRAS, 397, 757
Greaves J. S. et al., 2014, MNRAS, 438, L31
Grinsted A., Moore J. C., Jevrejeva S., 2004, Non-linear Process. Geophys., 11, 561
Gyenge N., Ludmány A., Baranyi T., 2016, ApJ, 818, 127
Hall J. C., Lockwood G. W., 1995, ApJ, 438, 404
Hall J. C., Lockwood G. W., Skiff B. A., 2007, AJ, 133, 862
Henry G. W., 1999, PASP, 111, 845
Howard A. W., Fulton B. J., 2016, PASP, 128, 1
Howe R., Christensen-Dalsgaard J., Hill F., Komm R. W., Larsen R. M., Schou J., Thompson M. J., Toomre J., 2000, Science, 287, 2456
Isaacson H., Fischer D., 2010, ApJ, 725, 875
Karak B. B., Mandal S., Banerjee D., 2018, ApJ, 866, 17
Katsova M. M., Kitchatinov L. L., Moss D. L., Olah K., Sokoloff D. D., 2018, Astron. Rep., 62, 72
Kiss T. S., Gyenge N., Erdélyi R., 2018, Adv. Space Res., 61, 611
Lanza A. F., 2014, A&A, 572, L6
Lanza A. F., 2018, A&A, 610, A81
Lanza A. F. et al., 2009, A&A, 530, 193
McIntosh S. W. et al., 2015, Nature Commun., 6, 6491
Mendoza B., Velasco V. M., Valdés-Galicia J. F., 2006, Sol. Phys., 233, 319
Metcalfe T. S., Judge P. G., Basu S., Henry T. J., Soderblom D. R., Knoelker M., Rempel M., 2009, preprint (arXiv:0909.5464)

Metcalfe T. S., Basu S., Henry T. J., Soderblom D. R., Judge P. G., Knölker M., Mathur S., Rempel M., 2010, ApJ, 723, L213
Meyers S. D., Kelly B. G., O'Brien J. J., 1993, Mon. Weather Rev., 121, 2858
Montet B. T., Tovar G., Foreman-Mackey D., 2017, ApJ, 851, 116
Obridko V. N., Shelting B. D., 2007, Adv. Space Res., 40, 1006
Olah K., Kovari Zs., Petrovay K., Soon W., Baliunas S., Kollath Z., Vida K., 2016, A&A, 590, A133
Poppenhaeger K., Wolk S. J., 2014, A&A, 565, L1
Radick R. R., Lockwood G. W., Henry G. W., Hall J. C., Pevtsov A. A., 2018, ApJ, 855, 75
Reinhold T., Cameron R. H., Gizon L., 2017, A&A, 603, A52
Reinhold T., Bell K. J., Kuszlewicz J., Hekker S., Shapiro A. I., 2018, A&A, in press
Salabert D. et al., 2016, A&A, 589, A118
Sanz-Forcada J., Stelzer B., Metcalfe T. S., 2013, A&A, 553, L6
Soon W. H., Baliunas S. L., Zhang Q., 1993, ApJ, 414, L33
Soon W., Frick P., Baliunas S., 1999, ApJ, 510, L135
Soon W. et al., 2014, Earth-Science. Reviews, 134, 1
Stefani F., Giesecke A., Weber N., Weier T., 2016, Sol. Phys., 291, 2197
Stefani F., Giesecke A., Weber N., Weier T., 2018a, Sol. Phys., 293, 12
Torrence C., Compo G., 1998, Bull. Am. Meteorol. Soc., 79, 61
Torrence C., Webster P. J., 1999, J. Clim., 12, 2679
Valdés-Galicia J. F., Velasco V. M., 2008, Adv. Space Res., 41, 297
Velasco Herrera V. M., Mendoza B., Velasco Herrera G., 2015, New Astron., 34, 221
Velasco Herrera V. M., Soon W., Velasco Herrera G., Traversi R., Horiuchi K., 2017, New Astron., 56, 86
Velasco Herrera V. M., Pérez-Peraza J., Soon W., Márquez-Adame J. C., 2018, New Astron., 60, 7
Wilson O. C., 1978, ApJ, 226, 379
Wilson O. C., 1968, ApJ, 153, 221
Zhang H., Bao S., 1998, A&A, 339, 880
Zhang H., Yang S., 2013, ApJ, 763, 105

APPENDIX A: HADAMARD MULTIPLICATION AND DIVISION OF MATRICES

In this Appendix, we list the formulas for the Hadamard multiplication and division of matrices, which consist of multiplying and dividing element by element. For example, if $\mathbf{A} = (a_{ij})$ and $\mathbf{B} = (b_{ij})$ are two m x n matrices then the Hadamard product ($\otimes$) and Hadamard division ($\ominus$) of $\mathbf{A}$ and $\mathbf{B}$ are the m x n matrices $\mathbf{C} = (c_{ij})$

$$\mathbf{A} \otimes \mathbf{B} = \begin{pmatrix} a_{11} & a_{12} & \cdots & a_{1n} \\ a_{21} & a_{22} & \cdots & a_{2n} \\ \vdots & \vdots & \ddots & \vdots \\ a_{m1} & a_{m2} & \cdots & a_{mn} \end{pmatrix} \otimes \begin{pmatrix} b_{11} & b_{12} & \cdots & b_{1n} \\ b_{21} & b_{22} & \cdots & b_{2n} \\ & & & \\ b_{31} & b_{32} & \ddots & \vdots \\ b_{m1} & b_{m2} & \cdots & b_{mn} \end{pmatrix}$$

$$= \begin{pmatrix} a_{11}b_{11} & a_{12}b_{12} & \cdots & a_{1n}b_{1n} \\ a_{21}b_{21} & a_{22}b_{22} & \cdots & a_{2n}b_{2n} \\ \vdots & \vdots & \ddots & \vdots \\ a_{m1}b_{m1} & a_{m2}b_{m2} & \cdots & a_{mn}b_{mn} \end{pmatrix}$$

$$= \begin{pmatrix} c_{11} & c_{12} & \cdots & c_{1n} \\ c_{21} & c_{22} & \cdots & c_{2n} \\ \vdots & \vdots & \ddots & \vdots \\ c_{m1} & c_{m2} & \cdots & c_{mn} \end{pmatrix} = \mathbf{C}$$

with

$$\mathbf{A} \otimes \mathbf{B} = \mathbf{B} \otimes \mathbf{A} = \mathbf{C}$$

Here, one may further note that the Hadamard product is not limited to multiplying between only two matrices. It is possible to multiply 'k' matrices with the condition that they all have the same number of rows and columns (m x n).

The Hadamard division ($\ominus$) for $\mathbf{A} = (a_{ij})$ and $\mathbf{B} = (b_{ij})$ is defined by $\mathbf{D}$ as

$$\mathbf{A} \ominus \mathbf{B} = \begin{pmatrix} a_{11} & a_{12} & \cdots & a_{1n} \\ a_{21} & a_{22} & \cdots & a_{2n} \\ \vdots & \vdots & \ddots & \vdots \\ a_{m1} & a_{m2} & \cdots & a_{mn} \end{pmatrix} \ominus \begin{pmatrix} b_{11} & b_{12} & \cdots & b_{1n} \\ b_{21} & b_{22} & \cdots & b_{2n} \\ & & & \\ b_{31} & b_{32} & \ddots & \vdots \\ b_{m1} & b_{m2} & \cdots & b_{mn} \end{pmatrix}$$

$$= \begin{pmatrix} \frac{a_{11}}{b_{11}} & \frac{a_{12}}{b_{12}} & \cdots & \frac{a_{1n}}{b_{1n}} \\ \frac{a_{21}}{b_{21}} & \frac{a_{22}}{b_{22}} & \cdots & \frac{a_{2n}}{b_{2n}} \\ \vdots & \vdots & \ddots & \vdots \\ \frac{a_{m1}}{b_{m1}} & \frac{a_{m2}}{b_{m2}} & \cdots & \frac{a_{mn}}{b_{mn}} \end{pmatrix} = \begin{pmatrix} d_{11} & d_{12} & \cdots & d_{1n} \\ d_{21} & d_{22} & \cdots & d_{2n} \\ \vdots & \vdots & \ddots & \vdots \\ d_{m1} & d_{m2} & \cdots & d_{mn} \end{pmatrix} = \mathbf{D}$$

In this paper, both cross-wavelet and wavelet coherence are calculated involving the procedures of Hadamard matrices multiplication and division, respectively.

In addition, we show in Fig. A1 the gapped cross-wavelet and gWTC spectra demonstrating the covariations of two artificial time series that only yield positive detection of the common implanted periodicities at 1.7 and 12 yr. This illustration adds confidence to the detection of the MTP for the chromospheric and photometric covariations at 1.6–1.8 yr shown in Fig. 4.

In Fig. A2, we show the real data example for the simultaneous detection/hint of the two rotational time-scales (i.e. 11 and 27 d) for solar activity records in order to offer support for our interpretation for the hint of two rotational modulations at 11 and 21 d for the gWTC spectra for the young solar analogue HD 30495 hinted in Figs 2 and 3 as well as discussed in the main text for the results from Fig. 4.

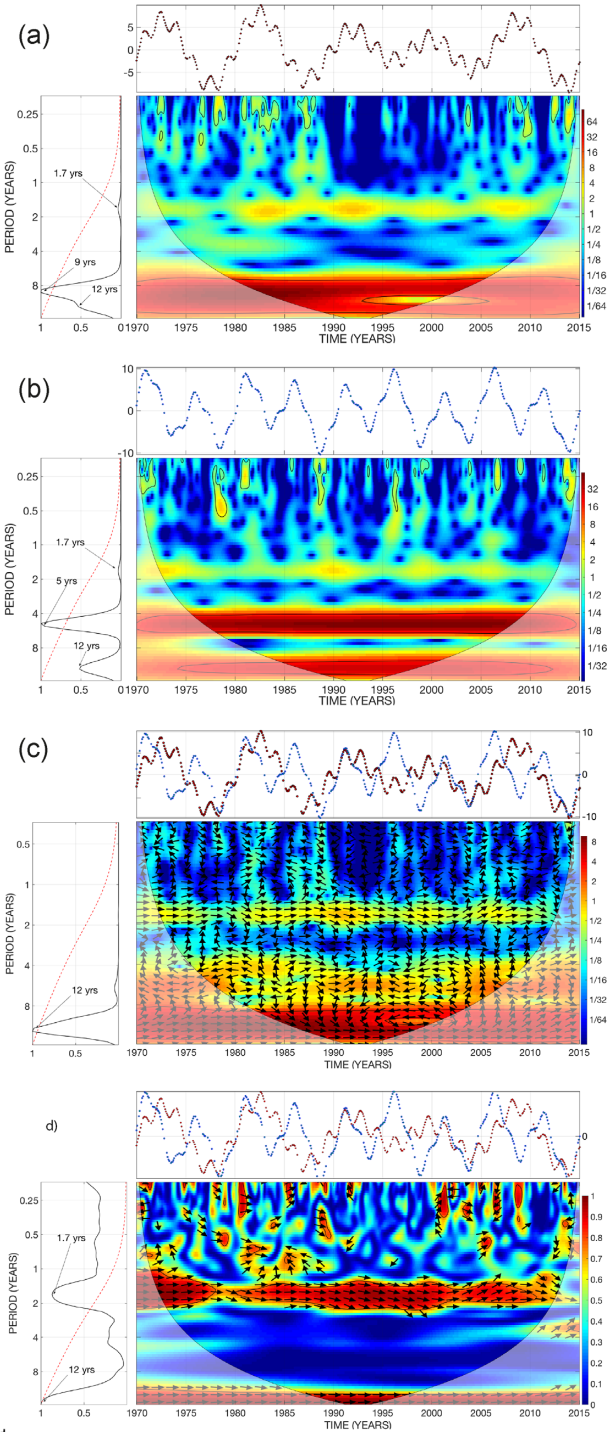

[htt .

Figure A1. Time–frequency wavelet coherency (WTC) and cross-wavelet spectrum of the covariations of two artificial test series with time-sampling gaps: (a) series A with periodic modulations at 1.7, 9, and 12 yr and (b) series B with periodic modulations at 1.7, 5, and 12 yr from 1970 to 2015. Panels (c) and (d) show the wavelet specturm for the gapped cross-wavelet and gWTC measures, respectively. Note that both the artificially implanted 1.7 and 12 yr oscillations are well detected in panels (c) and (d). We thus conclude that it is reasonable to infer from this test result that the mid-term 1.6–1.8 yr covarying scale detected in Fig. 4 is statistically real and physically meaningful.

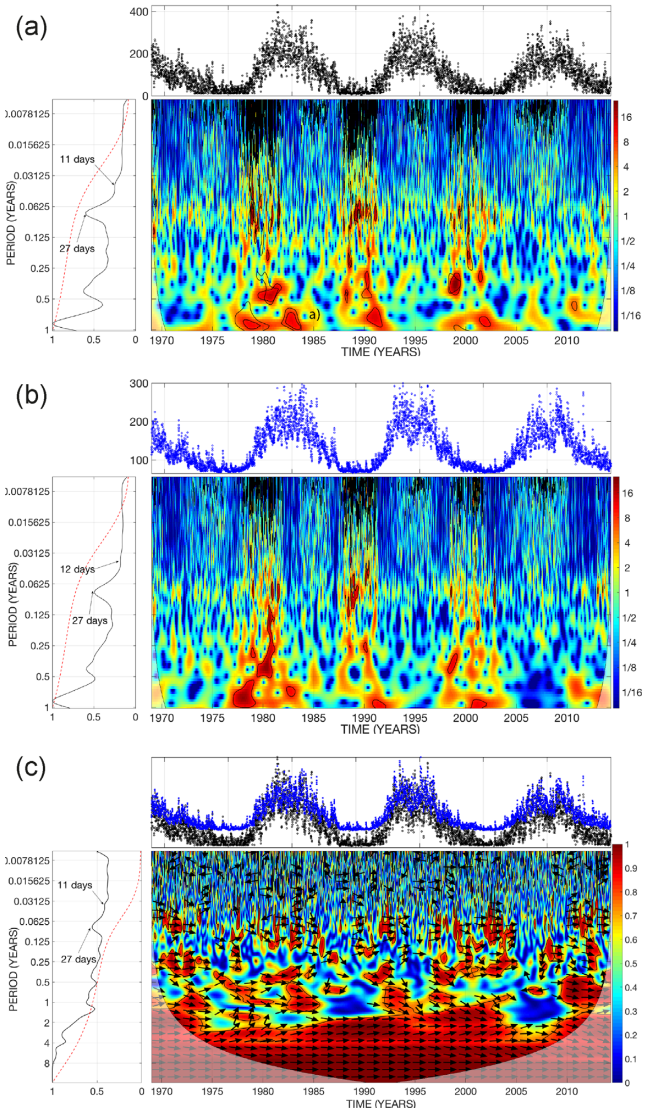

Figure A2. Gapped wavelet and gapped coherency (gWTC) spectrum of the covariations of (a) sunspot, (b) 10.7 cm solar radio flux series and wavelet coherence measure from 1970 to 2015, respectively. The result for this real-data example supports the hint in Fig. 4 for the detection of two simultaneous rotational time-scales at 11 and 21 d for young Sun HD 30495.

This paper has been typeset from a TEX/LATEX file prepared by the author.